

Feasibility of a Deep Direct-Use Geothermal System at the University of Illinois Urbana-Champaign

Andrew Stumpf¹, James Damico¹, Roland Okwen¹, Timothy Stark², Scott Elrick¹, W. John Nelson¹, Yongqi Lu¹, Franklin Holcomb³, James Tinjum⁴, Fang Yang¹, Scott Frailey¹, and Yu-Feng Lin¹

¹Illinois State Geological Survey, Prairie Research Institute,
University of Illinois at Urbana-Champaign, Champaign, IL

²Department of Civil and Environmental Engineering,
University of Illinois at Urbana-Champaign, Urbana, IL

³U.S. Army Engineer Research and Development Center,
Construction Engineering Research Laboratory, Champaign, IL

⁴College of Engineering,
University of Wisconsin-Madison, Madison, WI

Keywords

Illinois Basin, St. Peter Sandstone, Mt. Simon Sandstone, geologic models, geothermal modeling, deep direct-use, techno-economic simulation

ABSTRACT

This study assesses the feasibility of using deep direct-use (DDU) geothermal energy in agricultural research facilities on the University of Illinois at Urbana-Champaign campus to exploit low-temperature sedimentary basins, such as the Illinois Basin. Subsurface components of the system include extraction and injection wells and downhole pumps. Surface equipment includes heat pumps/exchangers, and fluid transport and monitoring systems.

Two geologic formations in the region exhibit a potential as sources for geothermal energy, based on pre initial temperatures and flow rates of fluids. The St. Peter and Mt. Simon Sandstones lie at depths of 634 and 1,280 m, respectively. Geocellular modeling is used to characterize the reservoirs. A St. Peter Sandstone model was made for an area south of the campus. Petrophysical and geothermal properties used are based on data from the closest wells

penetrating the formations. Characterization of the Mt. Simon Sandstone is in progress and is not discussed here.

Extraction and injection flows simulated with different wellbore configurations provide estimates of fluid flow out of and into the reservoir. The models are used to optimize flow rates, bottomhole pressure, and temperature of the produced fluid. Individual wellbore models simulate subsurface heat loss and gain, providing guidance on the optimal type and amount of insulation in the wellbore. Design of the surface facilities will address aspects of fluid delivery, heat exchange, capital operating costs, heat loss, and corrosion.

Heat capacity and flow rates are assessed to estimate life-cycle costs and benefits, including the environmental benefits of reducing greenhouse gases and water use and increased energy efficiency. A preliminary analysis of surface configurations for the DDU system (including cascading applications) based on building heat loads is being conducted to identify multiple system designs that will maximize performance, energy efficiency, and cost recovery.

1. Introduction

This study evaluates the feasibility of using deep direct-use (DDU) geothermal energy extracted from low-temperature geologic formations within the Illinois Basin (ILB) (Figure 1) to heat and cool agricultural research facilities located at the Energy Farm on the South Farms of the University of Illinois at Urbana-Champaign (U of IL) campus. The assessment site is located on a 90 km² area around the university campus in Champaign County, Illinois. Results of the reservoir property evaluations and reservoir thermal simulations will be used to design a geothermal system and evaluate its economic feasibility and environmental impacts. The results of the study will enable geothermal resources within the entire ILB to be more broadly assessed, and allow the technology to be extended to other geographical areas with similar low-temperature sedimentary basins and associated overlying end users (e.g., military installations, hospitals, and schools).

For the U of IL assessment, a doublet geothermal system with vertical and horizontal extraction and injections wells (Figure 2) is used in system simulations. The end-use facilities at the proposed research site provide a unique opportunity for DDU of geothermal heat at a reasonable scale. In the scenario, the wells are located within 1 km of each other and contain fluids at different temperatures. Heating load data at these facilities are being collected, and peak load versus base load and multiple heat applications will be identified. A preliminary analysis of different surface configurations for the geothermal energy system (including cascading applications of the spent formation fluid) will be conducted based on the heat load requirements to identify the most attractive DDU options in terms of performance, energy efficiency, and cost for the Energy Farm and other agricultural facilities in the area.

2. Geology

The geology in the 90 km² area of research (AOR) was characterized by using data from drilling records, wireline logs, and petrophysical analysis of core samples (Figure 1). However, the geology of the reservoirs is quite uncertain because few wells penetrate the target formations near the U of IL campus.

In Champaign County, thick deposits of Pleistocene glacial sediments completely mask the bedrock surface. The deposits range in thickness from less than 40 m to more than 120 m (Table 1). Below these deposits are sedimentary rocks that range in age from Cambrian through Pennsylvanian, with a total estimated thickness of roughly 1,525 m to more than 1,830 m. Precambrian metamorphic and igneous rocks underlie the sedimentary succession. The major geologic structure is the La Salle Anticlinorium (Figure 1), a belt of domes and anticlines that crosses Champaign County along a trend oriented northwest (Willman et al., 1975; Buschbach and Kolata, 1991; Kolata and Nimz, 2010). In 2016, the Illinois State Geological Survey drilled a shallow, continuously cored test hole at the proposed location for the geothermal system. This borehole penetrated 58 m of Pleistocene glacial sediments and 32 m of Pennsylvanian bedrock to a total depth of 90 m (McDaniel et al., 2018). Several Pennsylvanian marker units can be identified with virtual certainty, including the Herrin Coal, which lies at a depth of 63 to 66 m. Regional mapping of boreholes within and surrounding the site forms the basis for estimates of the depth and thickness of the intervening formations.

The St. Peter Sandstone and the basal Mt. Simon Sandstone were identified at an early phase of this investigation as having potential suitability for DDU geothermal applications. Leetaru (2014) described the Middle Ordovician St. Peter Sandstone as “a widespread, lithologically distinct, typically pure quartz arenite lithostratigraphic unit found throughout the upper Midwest, USA” (p. 20). Although exhibiting a high level of homogeneity in certain locations, the St. Peter Sandstone varies regionally because of diagenetic alteration, including calcite/dolomite cementation (Pitman et al., 1997). The Upper Cambrian Mt. Simon Sandstone is a pervasive formation through the entire ILB, which extends into Indiana, Iowa, Michigan, and western

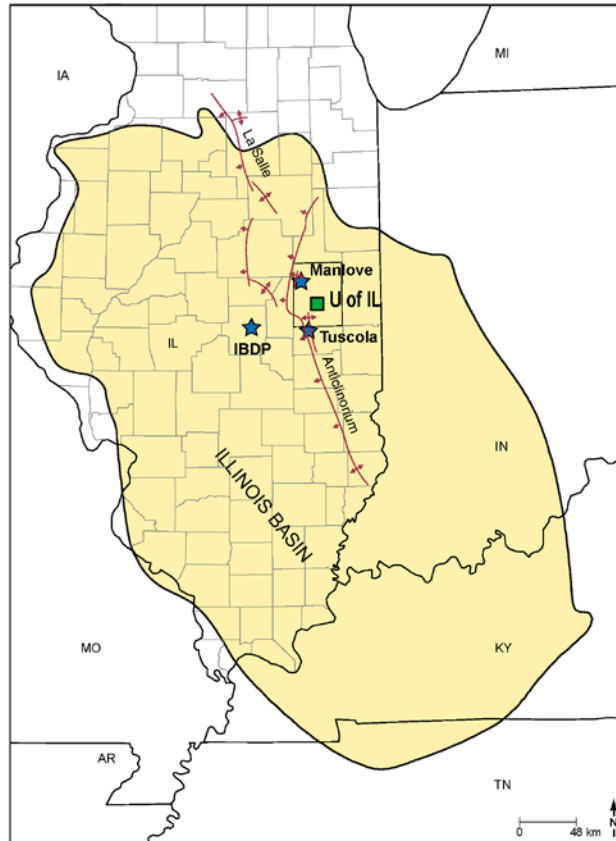


Figure 1. Location of the study site within the Illinois Basin in east-central Illinois. The basin is shaded in yellow and the study site is marked by a green box labeled U of IL. The Manlove and Tuscola gas storage fields and the CO₂ injection well located at the Illinois Basin–Decatur Project (IBDP) site are also denoted.

Kentucky. The sandstone has been correlated with formations in Missouri and Ohio (Morse and Leetaru, 2005). The formation is dominated by quartz-rich, very fine to coarse quartzose sandstone with sorting ranging from poorly to well sorted (Morse and Leetaru, 2005; Frailey et al., 2011). An arkosic sandstone with exceptionally good reservoir qualities is found regionally at the base (Frailey et al., 2011). Both formations are characterized by their high porosity and permeability. In certain portions, the formations serve as freshwater aquifers across the northern parts of Illinois as well as reservoirs for underground storage of natural gas in east-central Illinois (Morse and Leetaru, 2005). The Mt. Simon Sandstone has recently received considerable attention because of its potential as a target for sequestration of carbon dioxide (CO₂; Finley et al., 2011).

Table 1. Stratigraphy of geologic units at the Energy Farm on the U of IL campus.

Formation	Thickness (m)	Top (m)	Description of Formation
Quaternary	58	0	Silt, clay, sand, till; sand and gravel, water bearing
Pennsylvanian	46–61	58	Shale, siltstone, sandstone, coal beds
Mississippian	37–73	111	Largely siltstone; Chouteau Limestone at base
New Albany	21–27	162–177	Dark colored, hard shale
Grand Tower (Devonian)	21–27	186–201	Limestone, commonly sandstone at base
Silurian	189–207	210–229	Vuggy dolomite, lower part limestone; shows of oil likely
Maquoketa (Ordovician)	61	418	Shale; limestone in middle
Kimmswick	140	479	Limestone
Decorah and Platteville	300	521	Limestone, thin shale layers
Joachim	21	613	Dolomite and sandstone, shale layers
St. Peter	61–76	634	Pure quartz sandstone, water bearing
Knox Group	396	701	Dominantly dolomite, partly sandy and cherty
Ironton	46	1,097	Pure quartz sandstone, water bearing
Eau Claire	137	1,143	Shale, sandstone, and limestone; shale increasing downward
Mt. Simon	762+	1,280	Sandstone, commonly coarse grained; water bearing

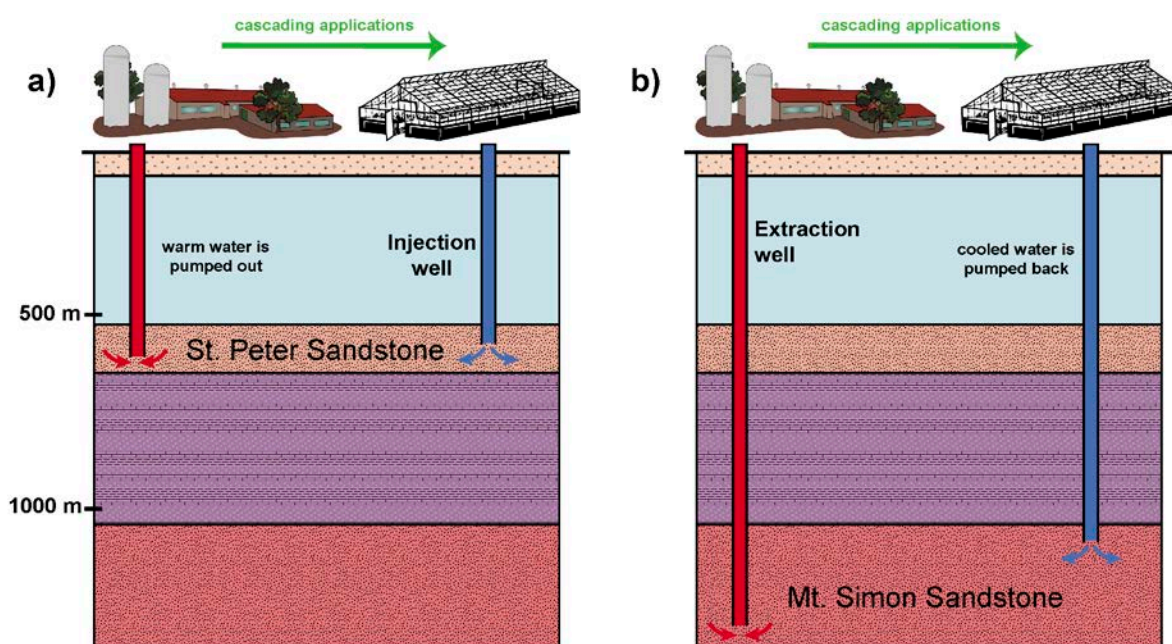


Figure 2. Conceptual diagram of the DDU geothermal system at the Energy Farm. A doublet well system consisting of a production well and injection well will be constructed in either the (a) St. Peter Sandstone or (b) Mt. Simon Sandstone. Geothermal fluids will be pumped from the reservoir through an extraction well, where at the surface they will be circulated through a heat recovery facility and then injected back underground into the same formation. The geothermal system will be used to heat and cool agricultural research facilities and greenhouses.

Within the 90 km² AOR, the St. Peter Sandstone is found at depths of 617.5 to 677.3 m, whereas the Mt. Simon Sandstone is encountered at depths of 1,329 to 2,031 m. The temperature of formation water in the St. Peter Sandstone within the AOR is estimated to range from 23.1 to 25.9 °C based on bottomhole temperatures from well logs and the temperature profile of a wireline log from the Illinois Basin–Decatur Project in nearby Macon County. Temperature estimates of the formation water in the deeper Mt. Simon Sandstone range from 36.9 to 49.8 °C. According to a regional study of brine and spring water samples, the salinity of the St. Peter Sandstone is estimated to range from 1,000 to 8,000 ppm, whereas the salinity of the Mt. Simon Sandstone is estimated at 50,000 to 115,000 ppm (Panno et al., 2018).

2.2 Geocellular Modeling

Current modeling and simulation efforts have focused on the St. Peter Sandstone. All model results presented in this paper are for only this formation. Modeling of the Mt. Simon Sandstone is ongoing. Although no deep boreholes penetrate the St. Peter Sandstone in the AOR, the formation is well characterized by several well logs and core analyses at two gas storage sites in Champaign County (Manlove and Tuscola) and by data from a CO₂ injection well at the IBDP site (Figure 1). At the Tuscola gas storage field, the site nearest the AOR, the upper third of the

St. Peter Sandstone is dolomitic (Bristol and Prescott, 1968). The Bristow #1 well has nearly 45.7 m of core samples collected at 0.3 m intervals that indicate heterogeneous reservoir properties within the St. Peter Sandstone (Figure 3). The average porosity was measured at 17.3%, whereas the average permeability was $2.18 \times 10^{-9} \text{ cm}^2$ (221 mD) (Table 2).

A geocellular static model for the St. Peter Sandstone in the AOR was constructed with Petrel[®] software from Schlumberger Limited. The model location is shown by the green box in Figure 1. The top and thickness of the St. Peter Sandstone were projected from regional analysis (Figure 4a & 4b). The model boundary was set at $10 \times 10 \text{ km}$ to overcome any potential boundary effects. The x and y grid spacing was 61 m, resulting in a grid with 159 cells in the x and y directions. The average thickness of the St. Peter Sandstone within the modeling area was 59 m and the number of layers was set at 39, resulting in an average layer thickness of 1.5 m.

The upper third of the St. Peter Sandstone in the region has a higher dolomite content, so the upper portion of the unit was modeled separately. Porosity was distributed by using the histogram of the core analysis data from the well at the Tuscola gas storage field. Permeability was back-transformed by using regression models built from the same core data and employing two separate models for the upper and lower parts of the formation (see Figure 5). Figures 6 and 7 show the distributions of porosity and permeability within the model.

Geothermal-specific properties, such as thermal conductivity, specific heat capacity, and the thermal expansion coefficient, were modeled as primarily a function of quartz content and temperature (Figures 8 and 9). Quartz content was estimated by using calculations from the apparent matrix time from the sonic log, assuming a binary mineral system of quartz and dolomite (cf. Asquith and Krygowski, 2006). The resulting statistics were used to inform the geostatistical distribution of quartz and dolomite content in the St. Peter Sandstone. Thermal conductivity (λ) could then be derived by using the equation from Robertson (1988):

$$\lambda = (\lambda_{\text{F}} + \gamma^2[(\lambda_{\text{S}} + \text{Qtz} * \text{S}) - \lambda_{\text{F}}]) \times 0.418 \text{ (W/[m}\cdot\text{K)]/ICU} \quad (1)$$

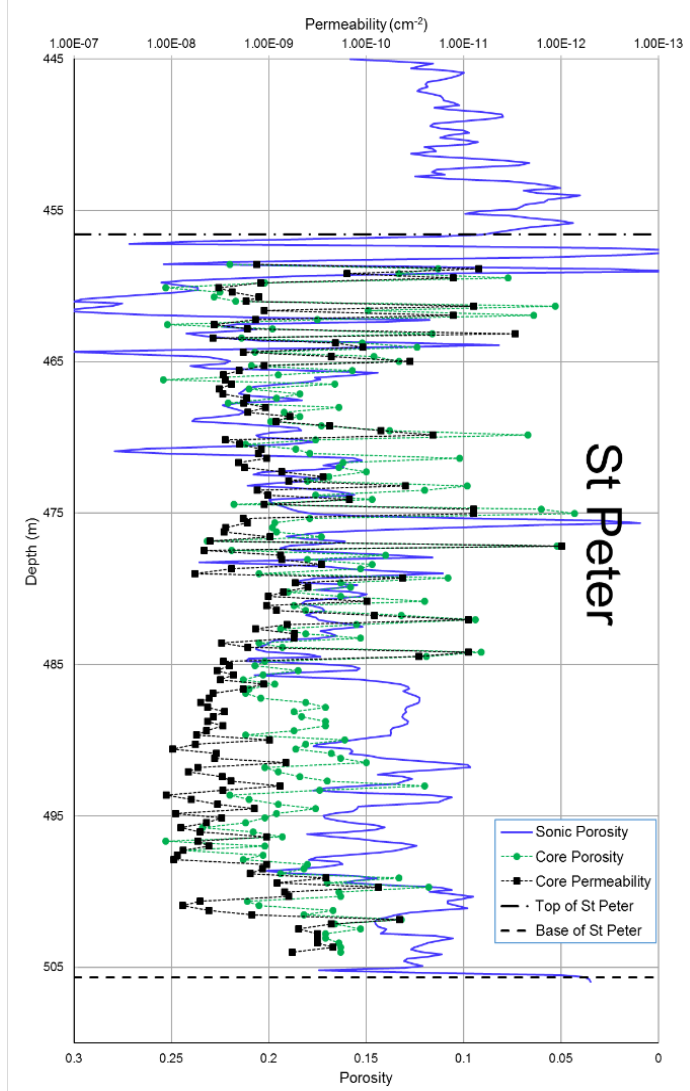


Figure 3. Petrophysical data for Bristow #1 well (Tuscola gas storage field ; API no. 120410071700, Sec. 4, 20N, 12W; Douglas County, Illinois).

where γ is the solidity of rock equal to $1 - \text{porosity}$, λ_F is the pore fluid thermal conductivity intercept at $\gamma^2 = 0$, λ_S is the solid rock thermal conductivity intercept at $\gamma^2 = 0$, Qtz is the percentage of quartz in the rock, and S is the slope constant (0.157 CU/percent for sandstone).

The specific heat capacity was calculated according to the methods developed by Waples and Waples (2004). First, the specific heat capacity was calculated by the proportions of sandstone and dolomite at 20 °C by using the following equation:

$$C_p = C_{pQ}Qtz + C_{pD}Dol \quad (2)$$

where C_p is the specific heat capacity of the rock, C_{pQ} is the specific heat capacity of quartz (740 J/kg·°C), Qtz is the percentage of quartz of the rock, C_{pD} is the specific heat capacity of dolomite (870 J/kg·°C), and Dol is the percentage of dolomite of the rock.

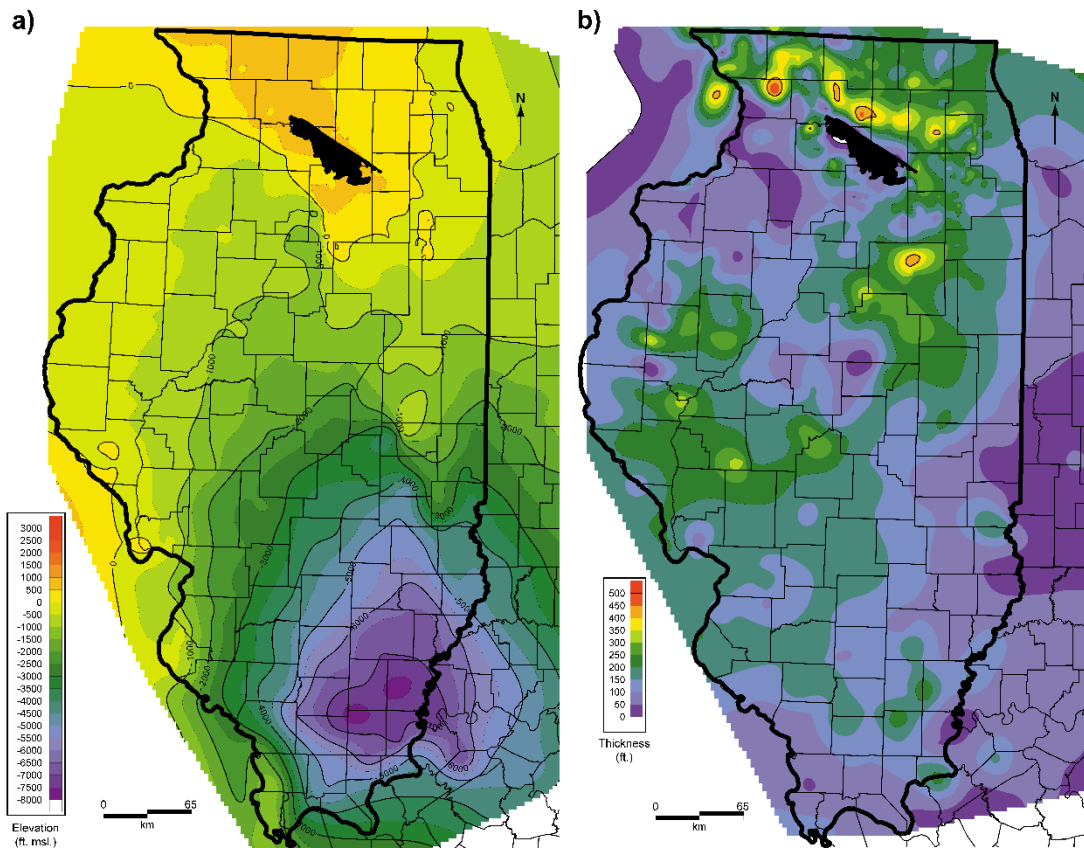


Figure 4. Structure contour maps of the St. Peter Sandstone for the (a) top surface elevation and (b) thickness (contours are in feet, where 1 ft = 0.3048 m). msl, mean sea level.

Because specific heat capacity is highly dependent on temperature, the specific heat capacity was adjusted from values at 20 °C to the ambient reservoir temperature by following the methodology recommended by Waples and Waples (2004). The normalized specific heat capacity (C_{pn}) was first calculated by using the following equation:

$$C_{pn} = 8.95 \times 10^{-10}T^3 - 2.13 \times 10^{-6}T^2 + 0.00172T + 0.716 \quad (3)$$

where T is the temperature ($^{\circ}\text{C}$). The C_{pn} was calculated for both reservoir temperature and 20°C , and then used to find the specific heat capacity at the reservoir temperature (C_{pT2}) by using the following equation:

$$C_{pT2} = C_{pT1} \times C_{pnT2}/C_{pnT1} \quad (4)$$

where C_{pT1} is the specific heat capacity at 20°C , C_{pnT2} is the normalized specific heat capacity at reservoir temperature, and C_{pnT1} is the normalized specific heat capacity at 20°C . Figures 8 and 9 show the resulting distribution of thermal conductivity and specific heat capacity. The coefficient of thermal expansion (α) is simply a product of mineral content, so a simple mixed model was used:

$$\alpha = \alpha_Q \text{Qtz} + \alpha_D \text{Dol} \quad (5)$$

where α_Q is the coefficient of thermal expansion of quartz and α_D is the coefficient of thermal expansion of dolomite.

The temperature (T , in $^{\circ}\text{C}$) was calculated from a depth-dependent equation derived from a temperature log measured at the IBDP site:

$$T = [(0.0101D + 54.632) - 32] \times 5/9 \quad (6)$$

where D is the depth in feet. Salinity was taken from a regional map of chloride concentration compiled by Panno et al. (2018), and these chloride values were converted to salinity.

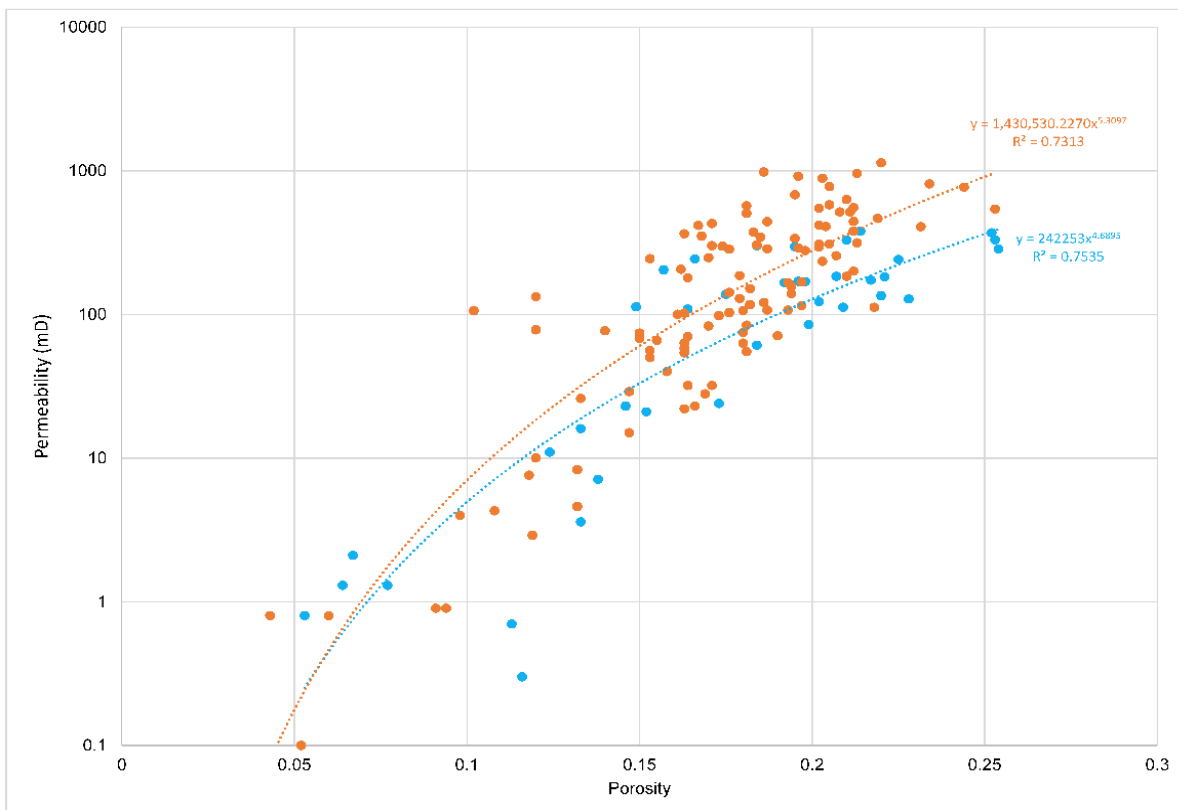


Figure 5. Porosity and permeability values plotted from core analysis data of the St. Peter Sandstone taken from the Bristow #1 well at the Tuscola gas storage field. Orange circles represent data from the lower part of the formation, and blue circles represent data from the upper part. The regression models are shown as well as dotted curved lines and are colorized according to the associated data. The resulting equation and coefficient of determination are also noted. Permeability is in millidarcies, where $1 \text{ mD} = 9.87 \times 10^{-9} \text{ cm}^2$.

Table 3 contains statistics of properties within the model. In comparison with data from the Tuscola gas storage field, the model averages for porosity and permeability were slightly lower; however, this result may partly be a function of an inherent bias in core analysis data toward higher quality reservoirs in petroleum and gas storage exploration. Porosity and permeability values have also been reported previously for the St. Peter Sandstone at the Manlove gas storage field located to the north of the AOR. At this site, the formation has average porosity and permeability values of 0.179 and $3.83 \times 10^{-9} \text{ cm}^2$ (388 mD), respectively (H.E. Leetaru, personal communication, April 14, 2018), illustrating the regional variation in reservoir quality. Walker et al. (2015) measured geothermal properties of the St. Peter Sandstone in Wisconsin and found λ was $3.45 \pm 0.67 \text{ W/m}\cdot\text{C}$ and C_p was $766 \pm 29.6 \text{ J/kg}\cdot\text{C}$, which fits well with our model averages. The static model provided the basis for dynamic reservoir modeling of the production and injection of geothermal fluids and wellbore modeling using dynamic modeling.

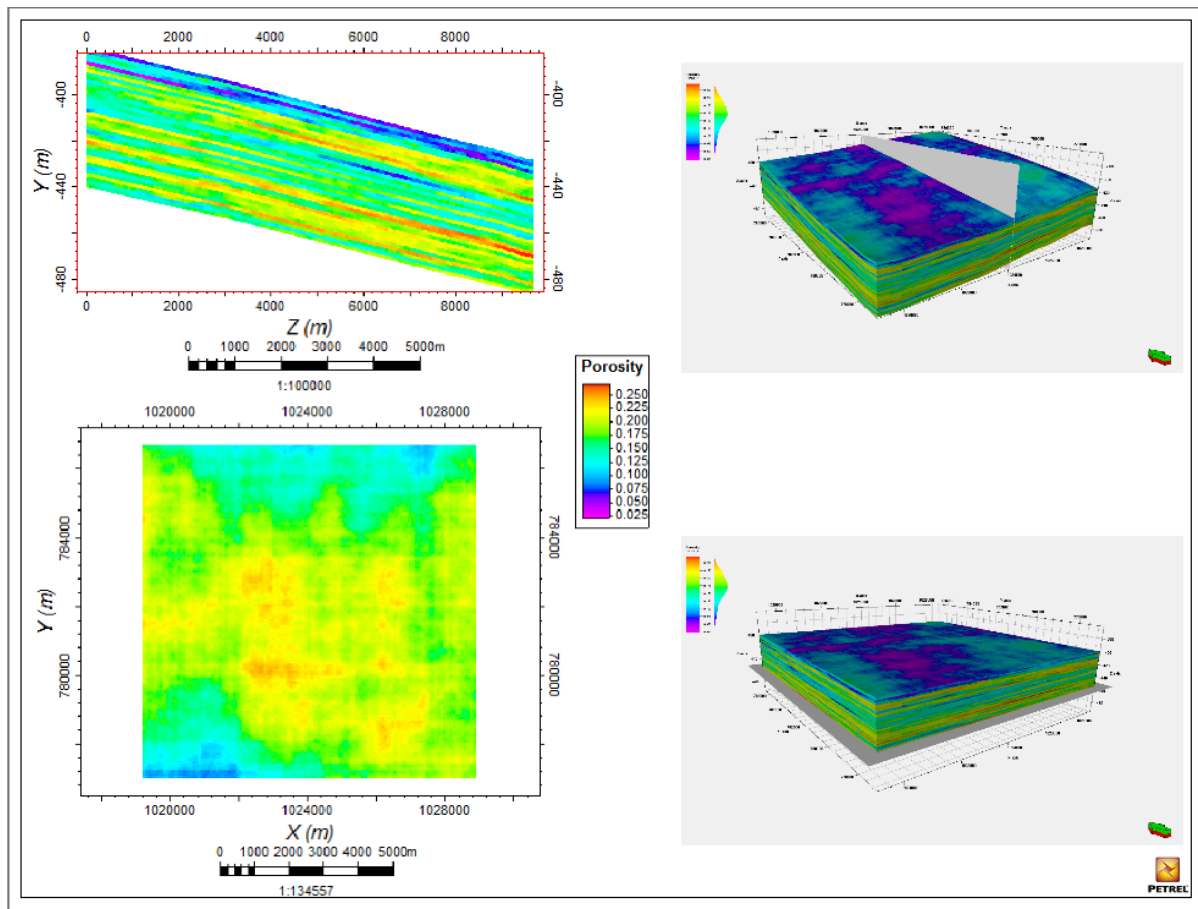


Figure 6. Distribution of porosity in the St. Peter Sandstone geocellular model. The image at the top left is a cross section oriented north to south, the location of which is shown by the white plane intersecting the model at the top right. The image on the bottom left is a plan view of one of the lower layers, the location of which is shown by the white plane intersecting the model at the bottom right. Vertical exaggeration is 25 \times .

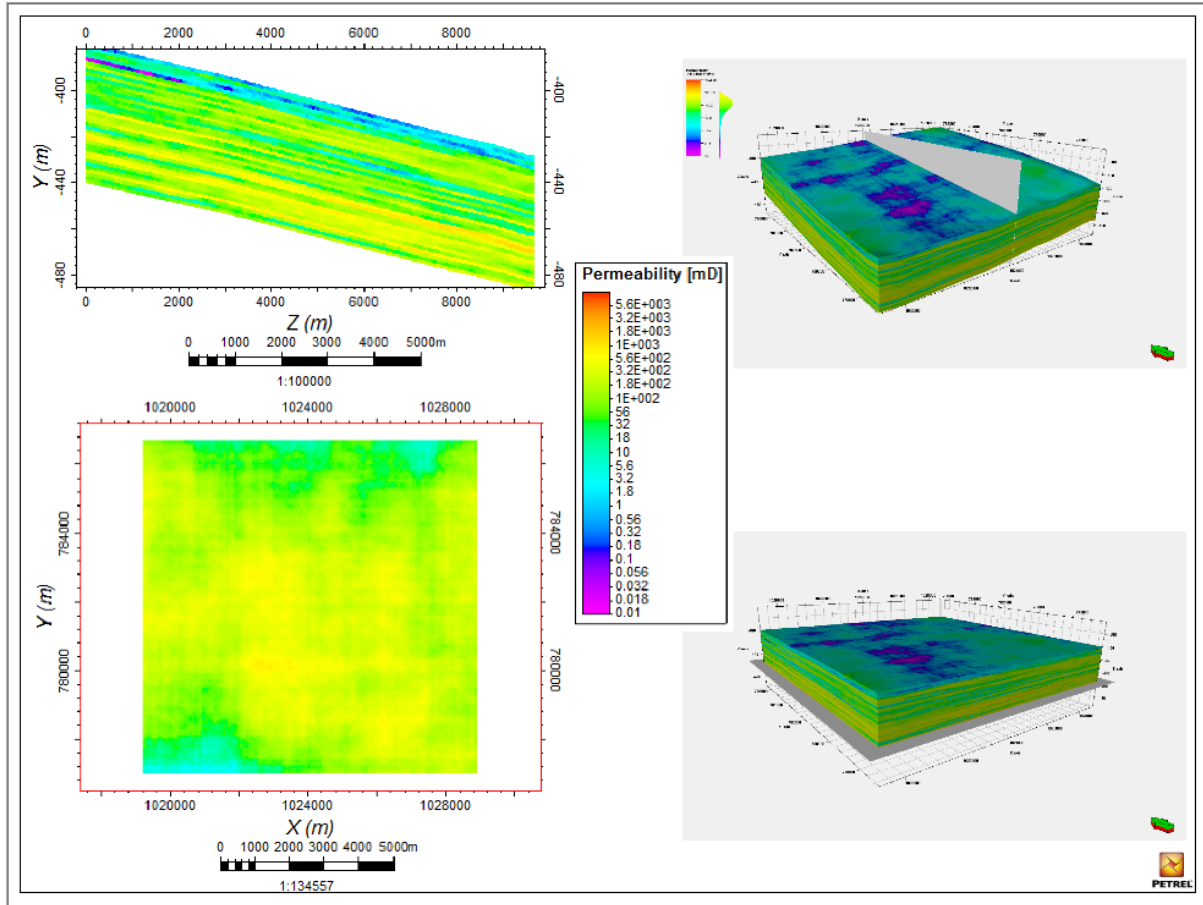


Figure 7. Distribution of permeability in the St. Peter Sandstone geocellular model. The image at the top left is a cross section oriented north to south, the location of which is shown by the white plane intersecting the model in the image at the top right. The image at the bottom left is a plan view of one of the lower layers, the location of which is shown by the white plane intersecting the model in the image at the bottom right. Vertical exaggeration is 25×.

Table 2. Core analysis data on porosity and permeability of St. Peter Sandstone from the Bristow #1 well.

Statistic	Core Porosity	Core Permeability (cm ²) [mD]
Min.	0.043	9.87×10^{-13} (0.1)
Max.	0.254	1.12×10^{-8} (1,140)
Mean	0.174	2.18×10^{-9} (221)
Median	0.180	1.37×10^{-9} (139)
Std. dev.	0.0415	2.27×10^{-9} (230)

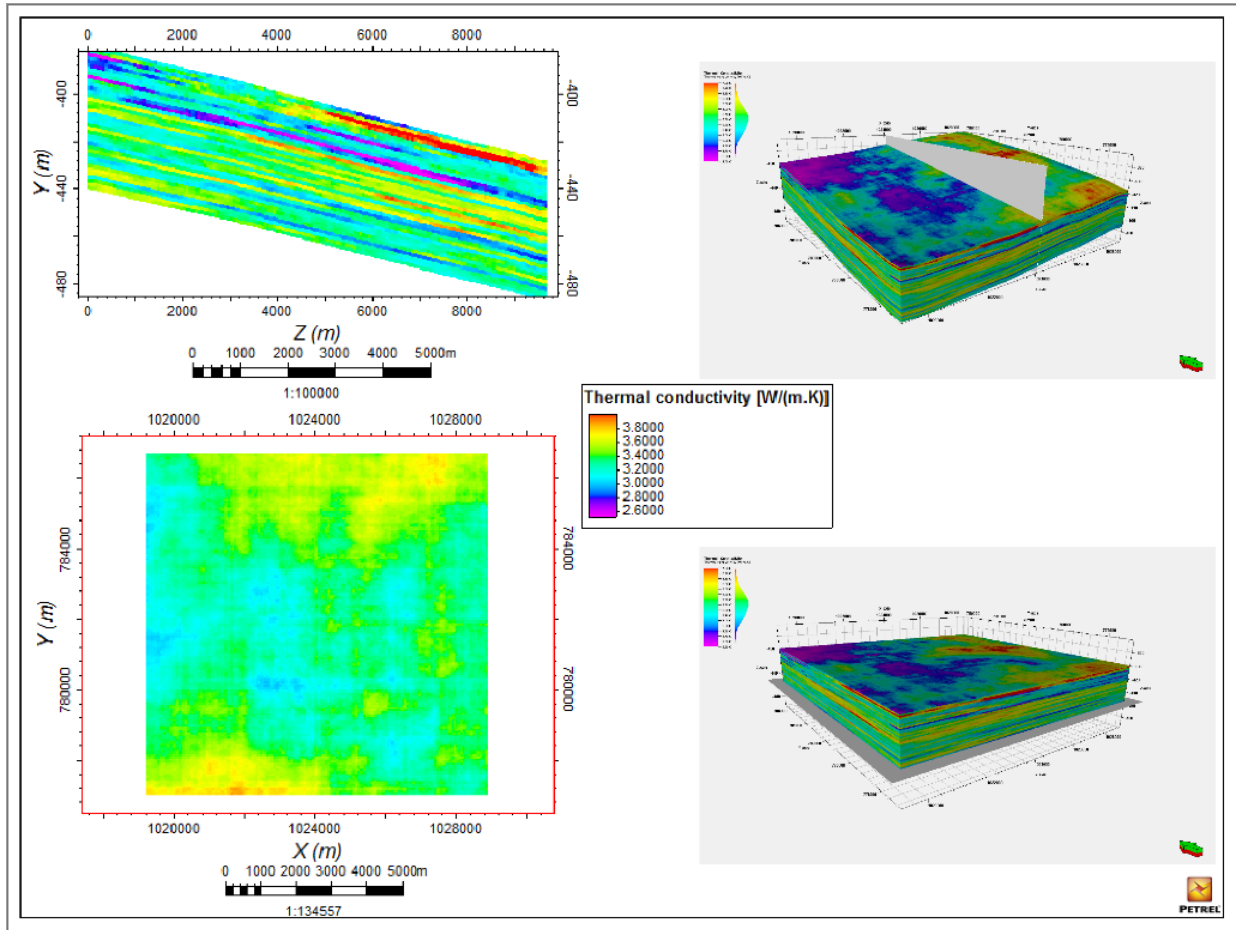


Figure 8. Distribution of thermal conductivity in the St. Peter Sandstone geocellular model. The image at the top left is a cross section oriented north to south, the location of which is shown by the white plane intersecting the model in the image at the top right. The image at the bottom left is a plan view of one of the lower layers, the location of which is shown by the white plane intersecting the model in the image at the bottom right. Vertical exaggeration is 25×.

Table 3. Properties of St. Peter Sandstone from the geocellular model.

Statistic	Porosity	Permeability (cm ²) [mD]	λ (W/m·°C)	Cp (J/kg·°C)	α ($\times 10^{-5}$ 1/°C)	Temperature (°C)	Salinity (ppm)
Min.	0.0224	4.34×10^{-14} (0.004)	2.17	745	3.20	23.1	2,264
Max.	0.270	1.33×10^{-8} (1350)	4.65	826	4.98	25.9	3,971
Mean	0.167	1.61×10^{-9} (163)	3.30	764	4.61	24.6	3,127
Median	0.171	9.71×10^{-10} (98.3)	3.30	760	4.70	24.6	3,137
Std. dev.	0.0452	1.83×10^{-9} (185)	0.284	15	0.337	0.48	488.1

3. Geothermal Modeling

3.1 Reservoir Model

Reservoir simulations for the St. Peter and Mt. Simon Sandstones are underway to establish the parameters needed to design the geothermal system. Preliminary geothermal reservoir simulations were completed using a generic homogeneous model to study the temperature distribution during fluid extraction and injection operations when using a doublet geothermal system. The model dimensions and average reservoir properties are presented in Table 4.

A $1,525 \times 1,555 \times 152$ m homogeneous model having a constant porosity and permeability of 20% and $9.9 \times 10^{-10} \text{ cm}^2$ (100 mD) was constructed to perform the preliminary geothermal reservoir simulations. The number of cells assigned to the x-, y-, and z-axes were 100, 101, and 100, respectively. Two wells, 1 km apart, were located on the opposite ends of the central column of the model. Equal volumes of fluid were extracted and then injected into the reservoir.

The maximum bottomhole pressure modeled during injection was 27,600 kPa (276 bar) at a depth of 1,524 m, based on a pressure gradient of 1.65 kPa/m. The modeled reservoir was

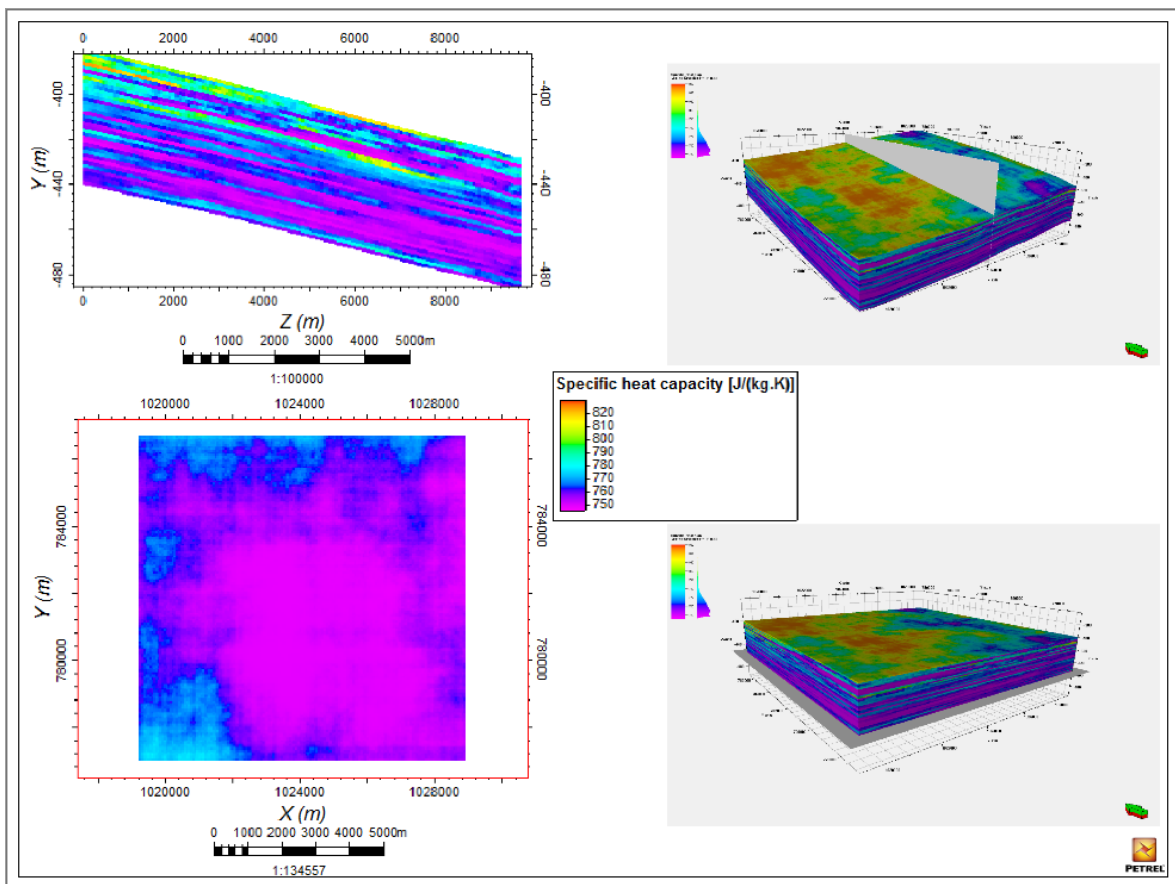


Figure 9. Distribution of specific heat capacity of the St. Peter Sandstone in the geocellular model. The image at the top left is a cross section oriented north to south, the location of which is shown by the white plane intersecting the model in the image at the top right. The image at the bottom left is a plan view of one of the lower layers, the location of which is shown by the white plane intersecting the model in the image at the bottom right. Vertical exaggeration is 25 \times .

assumed homogeneous when in thermal and hydrostatic equilibrium. Fluid was extracted at a temperature of 43 °C and injected at 10 °C. The flow rates in the extraction and injection wells were held constant at 159 m³/day (1,000 bbl/day) during the modeling. The simulations were run until the cool-water front reached the production well. Fluid was extracted from the bottom and injected at the top of the model because the temperature is higher at the bottom of the reservoir than at the top.

The results of the simulations indicate that the cool-water front generated during surface injection will not reach the extraction well within 50 years of operation (Figure 10). However, the injected colder water will reach the bottom of the formation within 20 years.

3.2 Wellbore Model

3.2.1 Introduction of Wellbore Modeling

A preliminary two-dimensional axisymmetric multi-physics wellbore model was constructed with the software package COMSOL Multiphysics[®] (v5.3) by COMSOL, Inc. to study the heat loss or gain through the wellbores during extraction and injection of fluid. Navier–Stokes heat conduction and heat convection equations were run to model the fluid flow and heat transfer, respectively, along the wellbores. A nine-formation model was developed (see Figure 11a). The types of tubing, annulus fluid, casing, and grout were considered in the model (see Figure 11b). Each wellbore reaches a depth of 630 m, and wells are spaced 50 m apart. The hydraulic and thermal properties of each formation were compiled and input in the model. These parameters are shown in Table 5. For the preliminary modeling, freshwater values were used as the transmitting fluid (see Table 6) because of the relatively lower salinity of the St. Peter Sandstone. For this modeling, all wellbore properties, geologic materials, and circulating fluids were assumed independent of temperature. The finite element mesh of the model was generated by using mapped structured quadrilateral elements having 29,323 cells.

Table 4. Properties of the generic reservoir based on the St. Peter Sandstone used in the preliminary geothermal simulation.

Parameter (unit)	Value
Porosity (%)	20
Permeability (cm ²) [mD]	
Horizontal	9.9×10^{-10} (100)
Vertical	4.4×10^{-10} (45)
Thickness (m)	152
Length (m)	1,524
Width (m)	1,676
Δx (m)	15
Δy (m)	15
Δz (m)	1.5
Dimensions (Nx:Ny:Nz)	100 × 101 × 100
Depth (m)	1,524
Reservoir temperature (°C)	43
Surface temperature (°C)	16
Reference rock specific heat capacity (J/kg·°C)	4,187
Reference thermal conductivity (W/m·°C)	41.54
Number of wells	2

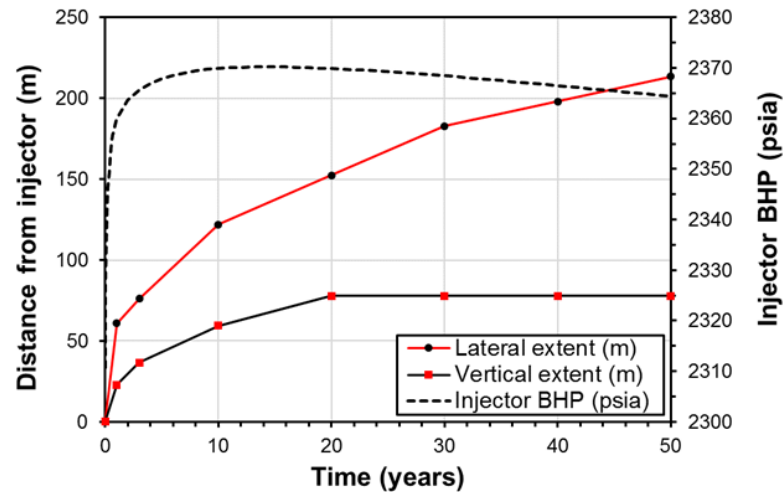


Figure 10. Projected temperature front location and bottomhole pressure (BHP) of the injection well at datum (1,525 m). 1 psia (pound per square inch absolute) = 6.89476 kPa.

3.2.2 Simulation Scenarios

The following scenarios are being simulated to provide a preliminary assessment of the sensitivity of the relevant wellbore design parameters.

1. Injection temperatures: Temperatures are being modeled from 21 to 27 °C and 6 to 16 °C for injection in the summer and winter seasons, respectively.
2. Injection and production rates: At present, the model includes flow rates of 0.9, 1.8, and 2.7 kg/s for the production and injection wells to investigate the influence of laminar and turbulent flow on heat loss.
3. Thermal conductivity: Thermal conductivity values of the geologic materials were input into the model as 0.1, 1.0, and 10 k_0 , where parameter k_0 (W/m·°C) represents the original thermal conductivity (Table 7).
4. Heat capacity: Specific heat capacity values for the geologic materials were input into the model as 0.1, 1.0, and 10 C_p , where parameter C_p (J/kg·°C) represents the original heat capacity (Table 7).
5. Insulation of wellbores: Fully insulated, uninsulated, and medium insulated conditions were simulated along the production wellbore. Heat loss in the injection well was not considered in this preliminary model. Three different types of grout and annulus fluid (Table 7) were tested to assess the effectiveness of the insulation in the three insulation cases outlined above in scenario 3.

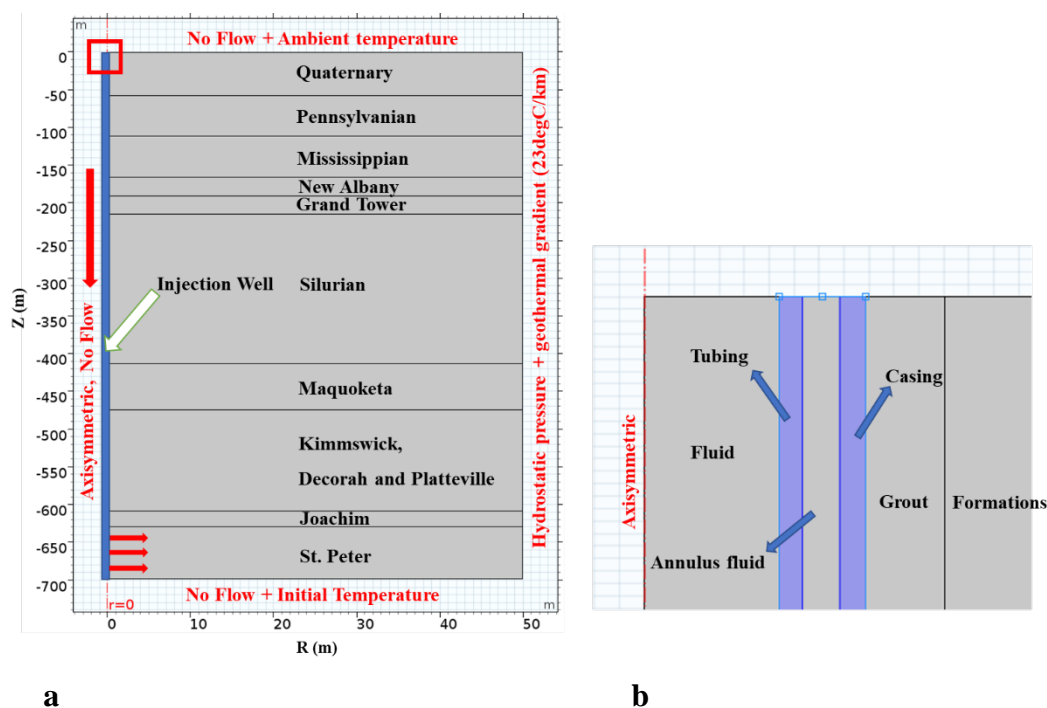


Figure 11. Wellbore geometry and boundary conditions. The (a) axisymmetric model with boundary conditions and (b) wellbore structures are shown.

Table 5. Thickness and properties of geologic materials.

Unit	Thickness (m)	Density (g/cm^3)	Porosity	Permeability (cm^{-2}) [mD]	Thermal Conductivity k_0 ($\text{W/m}\cdot^\circ\text{C}$)	Heat Capacity C_p ($\text{J/kg}\cdot^\circ\text{C}$)
Quaternary	58	1.50	0.30	1.0×10^{-9} (100)	1.5	1,500
Pennsylvanian	53	2.75	0.12	5.0×10^{-11} (5)	4.2	800
Mississippian	55	2.66	0.15	2.0×10^{-10} (20)	4.0	900
New Albany	24	2.54	0.20	1.0×10^{-13} (0.01)	2.3	879
Grand Tower	24	2.71	0.14	1.2×10^{-10} (12)	2.6	921
Silurian	198	2.80	0.12	1.0×10^{-10} (10)	4.5	879
Maquoketa	61	2.54	0.20	1.0×10^{-13} (0.01)	2.3	879
Kimmswick–Decorah and Platteville	134	2.71	0.14	1.0×10^{-10} (10)	2.6	921
Joachim	21	2.70	0.13	2.0×10^{-11} (2)	4.2	900

Table 6. Properties of water (at 20 °C and containing 4,000–5,000 ppm of dissolved solids).

Parameter (unit)	Value
Density (kg/m ³)	1,002
Viscosity (kg/m/s)	1.003×10^{-3}
Thermal conductivity (W/m·°C)	0.594
Heat capacity (J/kg·°C)	4,182

Table 7. Types and properties of wellbore elements for realistic insulation conditions.

Property	High insulation degree		Medium insulation degree		Low insulation degree		Tubing and casing
	Grout	Annulus fluid	Grout	Annulus fluid	Grout	Annulus fluid	
	Neat cement (w = 0.6)	Concentrated cesium and potassium formation brines	Thermally enhanced cementitious grout (w = 0.34, s/c = 2.0)	Concentrated sodium and potassium formation brines	Mix 111 (w = 0.55, s/c = 2.13)	Single-salt sodium formation brines	
Thermal conductivity (W/m·°C)	0.8	0.38	1.92	0.45	2.42	0.64	55
Density (g/cm ³)	14.5	18.4	15.9	14.2	18.2	10.0	65.5
Solid specific heat (J/kg·°C)	1,740	2,200	1,900	1,700	2,180	1,200	7,850

3.2.3 Preliminary Analysis

The results of the sensitivity analysis are shown in Figures 12 to 16. The preliminary modeling results regarding heat transfer in the wellbores are as follows:

- Heat loss or gain in the wells is primarily a function of the temperature difference between the borehole and surrounding formations and the thermal conductivity, creating a difference in outlet temperature of approximately 56% and 7.6%, respectively.

- The heat loss or gain in the production well is not significantly affected by changing flow rates and heat capacity values of the formations (<5% difference in the outlet temperature).
- Ordinary annulus fluids and grout insulation materials along the wellbores do not effectively retain heat in the production well; therefore, other types of insulation materials will be required to reduce the heat loss during extraction.
- The inversion point with zero (0) heat flux (i.e., the point at which the direction of heat transfer between the wellbore and formations reverses) occurs when the injection temperature ranges from approximately 10 to 27 °C. The depth of the inversion point increases with elevated injection temperatures and flow rates.

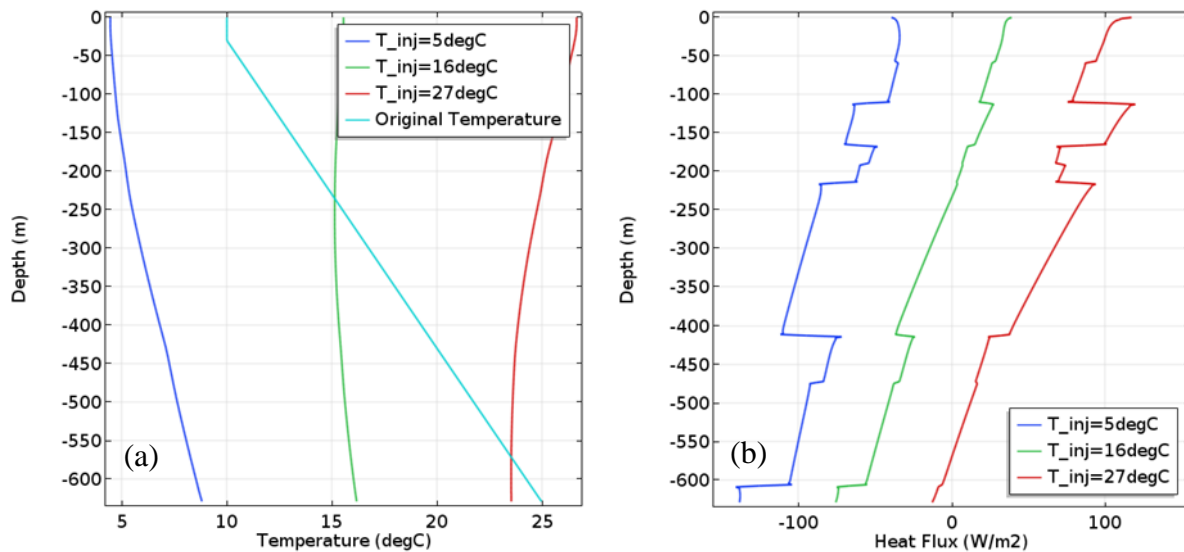


Figure 12. Thermal behavior with different injection temperatures (at a flow rate of 0.9 kg/s for 1 year). Shown are the (a) temperature profile along the wellbore (the light blue line represents the temperature of the surrounding formation) and (b) heat flux from the wellbore to the rock formations (positive).

4. Techno-Economic Simulation

Multiple methods are being applied to study the economic feasibility of DDU geothermal energy for agricultural uses on the U of IL campus as well as its environmental impact, which will primarily be measured by the offset in greenhouse gases released into the atmosphere. Six facilities at the study site that primarily obtain heat from a self-contained propane system, including three greenhouses, an office space, a maintenance shop, and a warehouse, were initially considered for geothermal heating. A preliminary economic analysis was conducted that included application of the simulation software tool GEOPHIRES[®] v2.0 (Beckers and McCabe, 2018). A large number of parameters were varied, including, but not limited to, (1) the energy use at the facilities, (2) the cost of constructing the extraction and injection wells, (3) the amount of heat available from the reservoirs, and (4) the cost of the propane fuel being replaced by the geothermal resource. A preliminary analysis of the life-cycle cost indicates running the geothermal system might not be the most cost-effective option at such a small scale. As a result,

the project is considering additional facilities for the geothermal system, which should improve the performance of the geothermal system relative to conventional systems because of economy of scale.

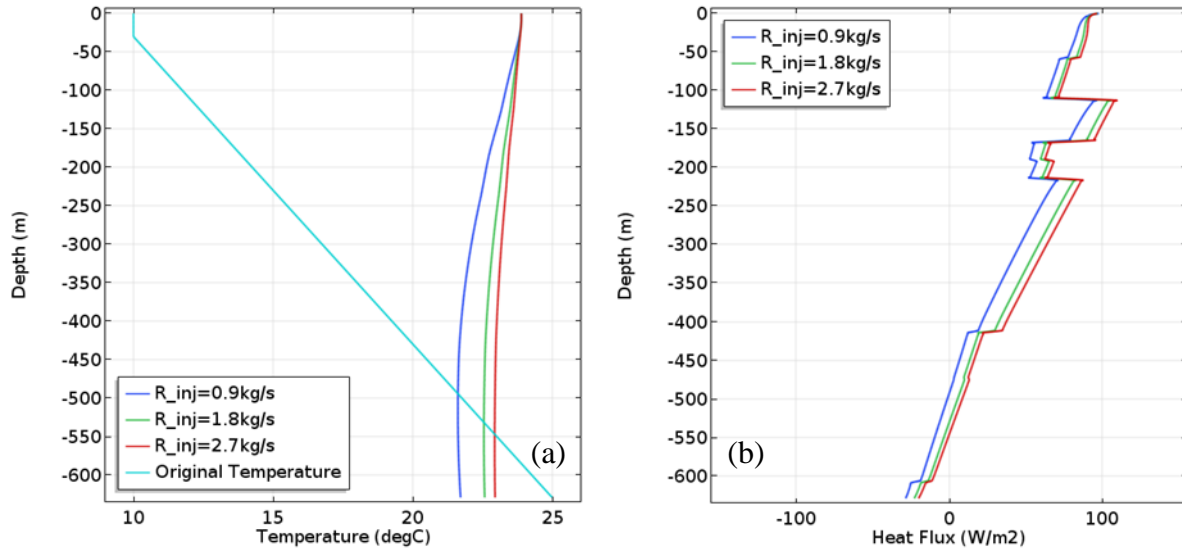


Figure 13. Thermal behavior with different flow rates (at an injection temperature of 24 °C for 1 year). Shown are the (a) temperature profile along the wellbore (the light blue line represents the temperature of the surrounding formation) and (b) heat flux from the wellbore to the rock formations (positive).

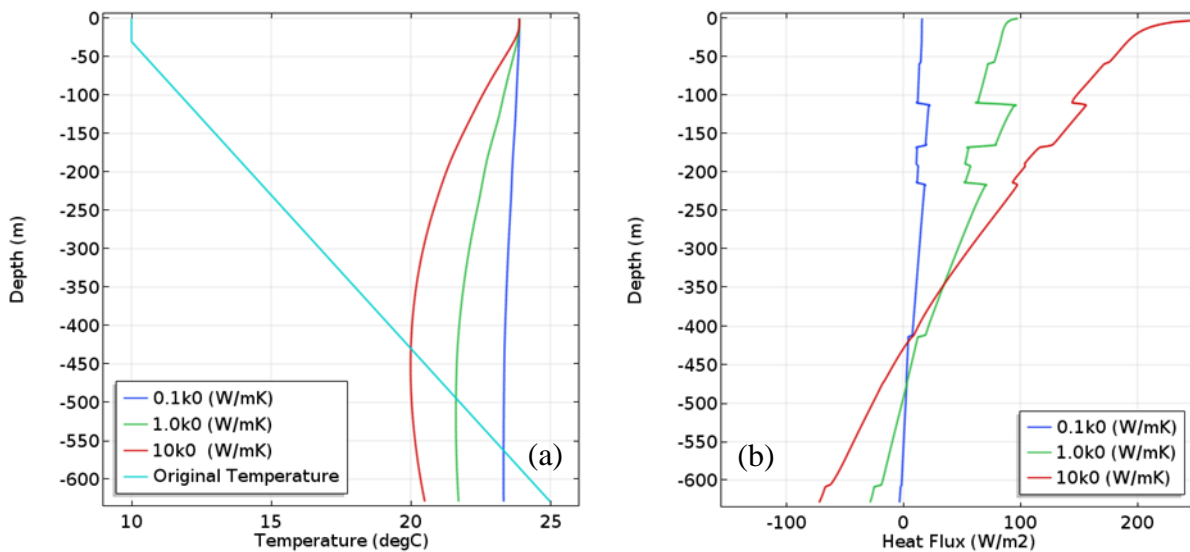


Figure 14. Thermal behavior with different rock formation thermal conductivity values (at an injection temperature of 24 °C with a flow rate of 0.9 kg/s for 1 year). Shown are the (a) temperature profile along the wellbore (the light blue line represents the temperature of the surrounding formation) and (b) heat flux from the wellbore to the rock formations (positive).

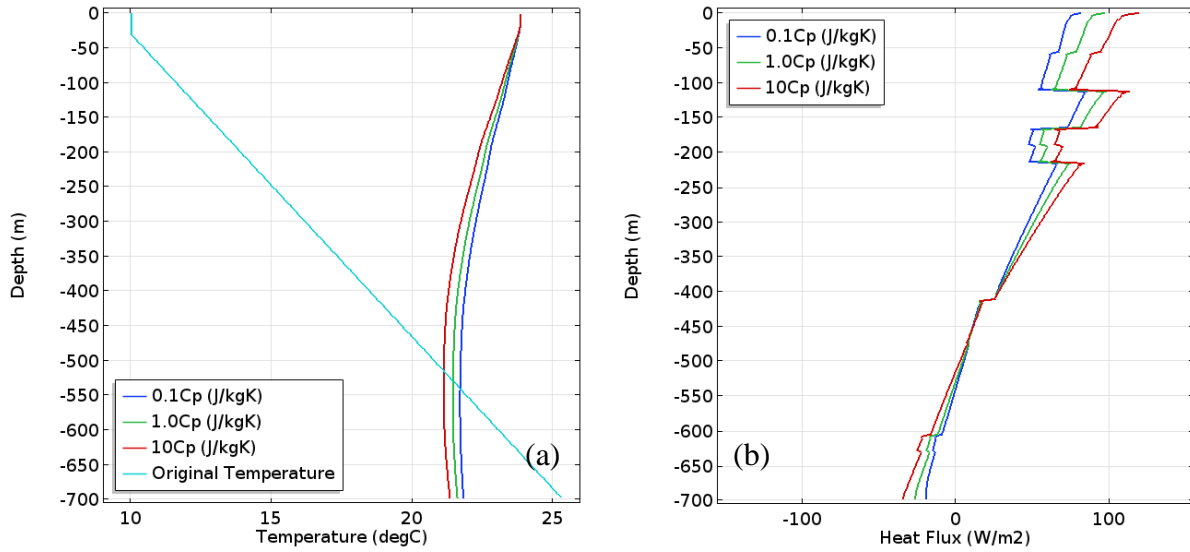


Figure 15. Thermal behavior with the different rock formation heat capacity values (at an injection temperature of 24 °C with a flow rate of 0.9 kg/s for 1 year). Shown are the (a) temperature profile along the wellbore (the light blue line represents the temperature of the surrounding formation) and (b) heat flux from the wellbore to the rock formations (positive).

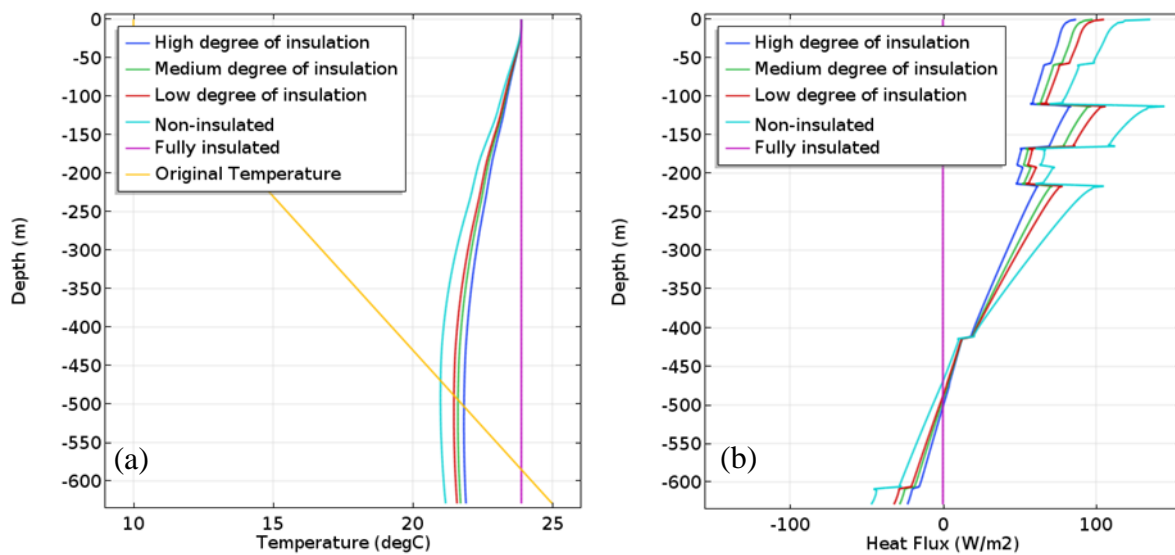


Figure 16. Thermal behavior with different insulation conditions (at an injection temperature of 24 °C with a flow rate of 0.9 kg/s for 1 year). Shown are the (a) temperature profile along the wellbore (the yellow line represents the temperature of the surrounding formation) and (b) heat flux from the wellbore to the rock formations (positive).

5. Conclusion

Integrated geological characterization and modeling, reservoir and wellbore modeling, and techno-economic simulations are being performed to determine the feasibility of using a DDU geothermal system to heat and cool agricultural facilities at the U of IL campus. Two widely distributed, water-bearing formations in the ILB, the St. Peter Sandstone and Mt. Simon Sandstone, are being investigated for their suitability as geothermal resources for DDU regionally. Geologic characterization indicates that the properties of the formations should be conducive to meeting the requirements for delivery of the fluid volumes needed for the DDU geothermal system. A high-resolution geocellular model of the St. Peter Sandstone reservoir architecture provided the basis for dynamic simulation of the reservoir behavior to exploit this geothermal resource. Reservoir simulations and wellbore modeling efforts are underway to determine the optimal well design and configuration. Preliminary techno-economic analyses provide a basis for continued assessment of the feasibility of DDU as additional applications of and needs for geothermal energy are determined on the U of IL campus. Initial results indicate that for the system to be economically efficient, it must be applied to a thermal demand load sufficient to justify the estimated drilling costs. Our ongoing efforts to identify different system designs that maximize performance, energy efficiency, and cost recovery will potentially be beneficial for broadening the development of DDU geothermal systems at other educational institutions and military installations within the ILB.

Acknowledgments

This material is based on work supported by the U.S. Department of Energy's Office of Energy Efficiency and Renewable Energy (EERE) under Geothermal Technologies Office Award Number DE-EE0008106.0000.

We acknowledge Hannes Leetaru for through editing and review of this paper as well as scientific input. Steve Whittaker also provided a constructive review. We acknowledge Charles Monson for his scientific input and for providing regional structure and isopach maps of the St. Peter Sandstone. Yaghoob Lasemi, Zohreh Askari Khorasgani, and Samuel Panno are acknowledged for their feedback and consultation. We also thank Damon Garner and Michelle Johnson for their assistance on the project. Edits to this submission by Arlene Anderson and Susan Krusemark are gratefully acknowledged.

We acknowledge Landmark Graphics for use of their software via the University Donation Program, Schlumberger, Ltd. for donation of the PetrelTM E&P software platform, and IHS for use of their Petra geological interpretation software via the University Grant Program.

Disclaimer

This report was prepared as an account of work sponsored by an agency of the United States Government. Neither the United States Government nor any agency thereof, nor any of their employees, makes any warranty, express or implied, or assumes any legal liability or responsibility for the accuracy, completeness, or usefulness of any information, apparatus, product, process disclosed, or represents that its use would not infringe privately owned rights.

Reference herein to any specific commercial product, process, or service by trade name, trademark, manufacturer, or otherwise does not necessarily constitute or imply its endorsement, recommendation, or favoring by the United States Government or any agency thereof. The views and opinions of authors expressed herein do not necessarily state or reflect those of the United States Government or any agency thereof.

REFERENCES

- Asquith, G., and Krygowski, D. *Basic Well Log Analysis*. American Association of Petroleum Geologists, Tulsa, OK (2006), 244 p.
- Beckers, K.F., and McCabe, K. “Introducing GEOPHIRES v2.0: Updated Geothermal Techno-Economic Simulation Tool.” *Proceedings: 43rd Workshop on Geothermal Reservoir Engineering*, Stanford University, Stanford, CA (2018), SGP-TR-213, p. 1–7, <https://pangea.stanford.edu/ERE/db/GeoConf/papers/SGW/2018/Beckers.pdf>.
- Bristol, H.M., and Prescott, R. “Geology and Oil Production in the Tuscola Area, Illinois.” Illinois State Geological Survey, Champaign, IL, Circular 424 (1968), 34 p., <http://hdl.handle.net/2142/45017>.
- Buschbach, T.C., and Kolata, D.R. “Regional Setting of Illinois Basin.” In Leighton, M.W., Kolata, D.R., Oltz, D.F., and Eidel, J.J., eds., *Interior Cratonic Basins*. American Association of Petroleum Geologists, Tulsa, OK, Memoir 51 (1991), p. 29–55, <https://pubs.geoscienceworld.org/books/book/1351/chapter/107171640/regional-setting-of-illinois-basin>.
- Frailley, S.F., Damico, J.R., and H.E. Leetaru. “Reservoir Characterization of the Mt. Simon Sandstone, Illinois Basin, USA.” *Energy Procedia*, 4 (2011), 5487–5494, <http://dx.doi.org/10.1016/j.egypro.2011.02.534>.
- Finley, R.J., Greenberg, S.E., Frailley, S.M., Krapac, I.G., Leetaru, H.E., and Marsteller, S. “The Path to a Successful One-Million Tonne Demonstration of Geological Sequestration: Characterization, Cooperation, and Collaboration.” *Energy Procedia*, 4 (2011), 4770–4776, <https://doi.org/10.1016/j.egypro.2011.02.441>.
- Kolata, D.R., and Nimz, C.K. *Geology of Illinois*. Illinois State Geological Survey, Champaign, IL (2010), 530 p.
- Leetaru, H.E. “An Evaluation of the Carbon Sequestration Potential of the Cambro-Ordovician Strata of the Illinois and Michigan Basins.” Illinois State Geological Survey, Champaign, IL, U.S. DOE Contract No. DE-FE0002068 (2014), 83 p., <https://doi.org/10.2172/1167490>.
- McDaniel A., Tinjum J., Hart D., Lin Y-F., Stumpf A., Thomas L. “Distributed Thermal Response Test to Analyze Thermal Properties in Heterogeneous Lithology.” *Geothermics*, 76 (2018), 116–124, <https://doi.org/10.1016/j.geothermics.2018.07.003>
- Morse, D.G., and Leetaru, H.E. “Reservoir Characterization and Three-Dimensional Models of Mt. Simon Gas Storage Fields in the Illinois Basin.” Illinois State Geological Survey, Champaign, IL, Circular 567 (2005), 72 p., <http://hdl.handle.net/2142/73423>.

- Panno, S.V., Askari, Z., Kelly, W.R., Parris, T.M., and Hackley, K.C. “Recharge and Groundwater Flow within an Intracratonic Basin, Midwestern United States.” *Groundwater*, 56 (2018), 32–45, <http://doi.org/10.1111/gwat.12545>.
- Pitman, J.K., Goldhaber, M.H., and Spötl, C. “Regional Diagenetic Patterns in the St. Peter Sandstone: Implications for Brine Migration in the Illinois Basin.” U.S. Geological Survey, Denver, CO, Bulletin 2094-A (1997), p. 1–17, <https://pubs.usgs.gov/bul/b2094a/b2094a.pdf>.
- Robertson, E.C. “Thermal Properties of Rocks.” U.S. Geological Survey, Reston, VA, Open-File Report 88-441 (1988), 106 p., <https://pubs.usgs.gov/of/1988/0441/report.pdf>.
- Walker, M.D., Meyer, L.L., Tinjum, J.M., and Hart, D.J. “Thermal Property Measurements of Stratigraphic Units with Modeled Implications for Expected Performance of Vertical Ground Source Heat Pumps.” *Geotechnical and Geological Engineering*, 33(2) (2015), 223–238, <https://doi.org/10.1007/s10706-015-9847-y>.
- Waples, D.W., and Waples, J.S. “A Review and Evaluation of Specific Heat Capacities of Rocks, Minerals, and Subsurface Fluids. Part 1: Minerals and Nonporous Rocks.” *Natural Resources Research*, 13(2) (2004), 97–122, <https://doi.org/10.1023/B:NARR.0000032647.41046.e7>.
- Willman, H.B., Atherton, E., Buschbach, T.C., Collinson, C., Frye, J.C., Hopkins, M.E., Lineback J.A., and Simon, J.A. “Handbook of Illinois Stratigraphy.” Illinois State Geological Survey, Champaign, IL, Bulletin 95 (1975), 261 p., <http://hdl.handle.net/2142/35115>.